Plasmonics (2014) 9:1163–1169
DOI 10.1007/s11468-014-9727-y

Systematic Theoretical Analysis of Selective-Mode Plasmonic Filter Based on Aperture-Side-Coupled Slot Cavity

Guangtao Cao · Hongjian Li · Yan Deng · Shiping Zhan · Zhihui He · Boxun Li

Received: 2 January 2014 / Accepted: 28 April 2014 / Published online: 13 May 2014

Abstract By taking the aperture as a resonator, we propose an analytical model to describe the dynamic transmission in metal-dielectric-metal (MDM) waveguide aperture-side-coupled with slot cavity. The theoretical results and the finite-difference time-domain (FDTD) simulations agree well with each other, and both demonstrate the mode selectivity and filtering tunability of the plasmonic structure. By adjusting the phase shifts in slot cavity or resonance frequency determined by the aperture, one can realize the required transmission spectra and slow light effect. The theoretical analysis may open up avenues for the control of light in highly integrated optical circuits.

Keywords Surface plasmon polariton · Plasmonic filter · Coupled-mode theory · Finite-difference time-domain method · Integrated optics devices

Introduction

Plasmonic waveguides have shown the considerable potential to transmit and manipulate light below the diffraction limit. Among the wide variety of plasmonic waveguide structures being investigated, metal-dielectric-metal (MDM) waveguides are of particular interest because they are easily fabricated and have deep subwavelength confinement of light with an acceptable propagation length for surface plasmon polaritons (SPPs) [1–7]. These remarkable advantages have motivated researchers to design and investigate various optical devices in plasmonic MDM waveguide platform, such as splitter [3, 8–11], bend [8, 12, 13], Y-shaped combiner [14], coupler [15, 16], Mach–Zennder interferometer [17], and switch [18–22].

As one of the most prevalent devices in optical circuits, plasmonic filters based on MDM waveguide have been studied widely, including tooth-shaped filter [23–25], multichannel filter [26, 27], channel drop filter with disk resonator [28], rectangular geometry resonator [29, 30], and ring resonator [31]. For the previous studies, 2D MDM-based resonant structures suitable for filtering purposes can be mainly categorized as ring resonator [31, 32], stub [23–25], and cavity [29, 30, 33]. Due to the tight mode confinement in MDM waveguide, resonator excitation via evanescent coupling is both inefficient and challenging to realize even with state-of-the-art electron beam or ion beam lithography. So, aperture coupling was proposed to realize effective coupling [34–37]. However, a systematic theoretical analysis is still lacking for the basic building blocks necessary for the manipulation of SPPs in MDM waveguide aperture-side-coupled with slot cavity.

In this paper, by taking the aperture as a resonator, a more detailed analytical theory for describing the dynamic transmission characteristics in plasmonic filter based on aperture-side-coupled slot cavity is proposed using the temporal coupled-mode theory (CMT) [38]. The consistence between the analytical model and the finite-difference time-domain (FDTD) method validates the feasibility of the theoretical analysis.

G. Cao · H. Li (✉) · S. Zhan · Z. He · B. Li
College of Physics and Electronics, Central South University, 410083 Changsha, People's Republic of China
e-mail: lihj398@126.com

G. Cao · H. Li
College of Materials Science and Engineering, Central South University, 410083 Changsha, China

Y. Deng
College of Physics, Mechanical and Electrical Engineering, Jishou University, 416000 Jishou, China

Analytical Model

Figure 1a is a schematic illustration of MDM bus waveguide aperture-side-coupled to slot cavity. The insulator and metal in the structure are air and silver, respectively. The permittivity of silver is characterized by Drude model $\varepsilon(\omega)=1-\omega_p^{\ 2}/(\omega^2+i\omega\gamma_p)$, with $\omega_p=1.38\times10^{16}$ rad/s and $\gamma_p=2.73\times10^{13}$ rad/s. These parameters are obtained by fitting the experimental results [39]. ω is the angular frequency of incident light. The main structure parameters are the width of bus waveguide, slot cavity and aperture (w), lengths of the left and right slot cavities to aperture center (L_1 and L_2), and the gap between the bus waveguide and slot cavity (g). When the TM polarization light is incident along x-axis, SPP wave can be formed on metal-insulator interfaces and confined in the waveguide. Here, the dynamic transmission characteristics of the proposed structure can be analyzed by the CMT, as illustrated in Fig. 1b. With the aperture center as a reference plane, the aperture is taken as a resonator. S_{+hn} and S_{-hn} (h, n=1, 2) stand for incoming and outgoing waves into the resonator. The temporal evolution of energy amplitude a of the resonator can be described as

$$\frac{\mathrm{da}}{\mathrm{dt}}=\left(j\omega_0-\frac{\omega_0}{Q_i}-\frac{\omega_0}{2Q_1}-\frac{\omega_0}{2Q_2}\right)a+S_{+21}e^{j\theta_0}\sqrt{\frac{\omega_0}{2Q_2}}+S_{+11}e^{j\theta_1}\sqrt{\frac{\omega_0}{2Q_1}}+S_{+12}e^{j\theta_2}\sqrt{\frac{\omega_0}{2Q_1}}+S_{+22}e^{j\theta_3}\sqrt{\frac{\omega_0}{2Q_2}}, \tag{1}$$

where Q_i, Q_1, and Q_2 are cavity quality factors related to intrinsic loss, slot cavity coupling loss, and waveguide coupling loss, respectively. ω_0 is resonant frequency of the resonator. θ_0 and θ_3 (θ_1 and θ_2) represent the phases of coupling coefficients between resonator and bus waveguide (slot cavity).

With the conservation of energy, we get

$$S_{-22}=S_{+21}-e^{-j\theta_0}\sqrt{\frac{\omega_0}{2Q_2}}a, \tag{2}$$

$$S_{-11}=S_{+12}-e^{-j\theta_1}\sqrt{\frac{\omega_0}{2Q_1}}a, \tag{3}$$

$$S_{-12}=S_{+11}-e^{-j\theta_2}\sqrt{\frac{\omega_0}{2Q_1}}a. \tag{4}$$

In the slot cavity, the wave satisfies the following relations: $S_{+11}=S_{-11}\sigma_1\exp(-j\varphi_1)$ and $S_{+12}=S_{-12}\sigma_2\exp(-j\varphi_2)$ ($0<\sigma_1$, $\sigma_2<1$). $\varphi_1=2\omega\mathrm{Re}(n_{\mathrm{eff}})L_1/c+\delta_1$ and $\varphi_2=2\omega\mathrm{Re}(n_{\mathrm{eff}})L_2/c+\delta_2$ (σ_1 and σ_2) are phase shifts (loss coefficients) of SPPs mode per round trip in left and right slot cavities of the reference plane, respectively. δ_1 and δ_2 are the phase shifts of SPPs mode reflected on the two ends of slot cavity. $\mathrm{Re}(n_{\mathrm{eff}})$ is the real part of effective index for SPPs in slot cavity [5, 18, 40]. With the boundary conditions of $S_{+22}=0$, we finally arrive at the transfer function of the system:

$$t=\frac{S_{-22}}{S_{+21}}=\frac{j\left(\frac{\omega}{\omega_0}-1\right)+\frac{1}{Q_i}+\frac{1}{2Q_1}-\frac{\frac{1}{2Q_1}\left[\frac{e^{j\phi_1}}{\sigma_1}+\frac{e^{j\phi_2}}{\sigma_2}+e^{j(\theta_1-\theta_2)}+e^{j(\theta_2-\theta_1)}\right]}{1-\frac{e^{j(\phi_1+\phi_2)}}{\sigma_1\sigma_2}}}{j\left(\frac{\omega}{\omega_0}-1\right)+\frac{1}{Q_i}+\frac{1}{2Q_1}+\frac{1}{2Q_2}-\frac{\frac{1}{2Q_1}\left[\frac{e^{j\phi_1}}{\sigma_1}+\frac{e^{j\phi_2}}{\sigma_2}+e^{j(\theta_1-\theta_2)}+e^{j(\theta_2-\theta_1)}\right]}{1-\frac{e^{j(\phi_1+\phi_2)}}{\sigma_1\sigma_2}}}. \tag{5}$$

According to Eq. 5, we can systematically analyze the spectra responses in the aperture-side-coupled nanostructure.

Simulation Results and Discussions

Figure 2a shows the transmission spectra from the same constructive parameters (w=100 nm, g=120 m, $L=L_1+L_2$=600 nm), yet with L_1=300, 250, 200, 140, 90, and 50 nm. The contour profiles of field H_z at different wavelengths, for L_1=200 nm, are depicted in Fig. 2b–d. For the plasmonic filter, the resonance modes are denoted by TM_m (m is the number of node of the standing waves in the slot cavity). Using the definition of resonance mode, we aim to investigate the evolution of transmission dips versus L_1. Figure 2b, d shows the z-component magnetic field distributions of transmission dips at λ=433 and 781.2 nm corresponding to TM_4 and TM_3 modes,

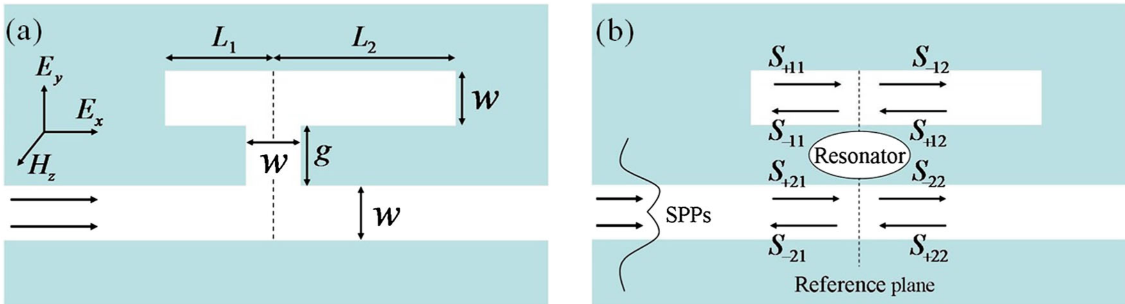

Fig. 1 **a** Schematic of the plasmonic filter. **b** Equivalent theoretical model for **a**

respectively. Figure 2c depicts the z-component magnetic field patterns at λ=553.3 nm. The results in Fig. 2b–d are in conformity with the transmission spectra in Fig. 2a. In Fig. 2a, the resonant wavelength of TM_4 mode (around 450 nm) oscillates with the variation of L_1, and the period P_4 is about 170 nm. The full width at half maximum (FWHM) for TM_4 mode is in the range of 11–14 nm, that is to say, it is nearly constant. For the TM_3 mode (around 550 nm), the evolution of resonant wavelength also exhibits periodicity with the change of L_1 from 300 to 50 nm, and the period P_3 is about 210 nm. As L_1=300 or 90 nm, the TM_3 mode is suppressed. The phenomenon for L_1= 300 nm has been attributed to the symmetry of plasmonic structure [37]. However, what gives rise to the disappearance of TM_3 mode for L_1=90 nm?

To gain a deep insight into physical mechanism of the phenomena discussed above, we will investigate the transmission spectra versus L_1 and λ by the CMT in the following. For simplicity, we set $\theta_1=\theta_2$ and $\sigma_1=\sigma_2$, then Eq. 5 can be expressed as

$$t=\frac{S_{-22}}{S_{+21}}=\frac{j\left(\frac{\omega}{\omega_0}-1\right)+\frac{1}{Q_i}+\frac{1}{2Q_1}-\frac{\frac{1}{2Q_1}\left[\frac{e^{j\phi_1}+e^{j\phi_2}}{\sigma}+2\right]}{1-\frac{e^{j(\phi_1+\phi_2)}}{\sigma^2}}}{j\left(\frac{\omega}{\omega_0}-1\right)+\frac{1}{Q_i}+\frac{1}{2Q_1}+\frac{1}{2Q_2}-\frac{\frac{1}{2Q_1}\left[\frac{e^{j\phi_1}+e^{j\phi_2}}{\sigma}+2\right]}{1-\frac{e^{j(\phi_1+\phi_2)}}{\sigma^2}}}. \tag{6}$$

Based on Eq. 6, we discuss the transmission responses $T=|t|^2$ versus L_1 and λ in Fig. 2e. For the theoretical model, ω_0=4.159×10^{15} rad/s, Q_i=300, $Q_1=Q_2$=20, σ=0.98, $\delta_1=\delta_2$= 0.6, and Re(n_{eff})=1.26. The periodicity of TM_4 and TM_3 modes is well presented. To exhibit the formation and evolution mechanisms of the transmission spectra more explicitly, in Fig. 2f, we show the top view of Fig. 2e. The periods for TM_4 (P_4) and TM_3 (P_3) modes are approximately equal to 180 and 210 nm, respectively. The small discrepancy between the FDTD simulations and theoretical results is due to the dispersion of the effective index n_{eff} for SPPs. With the variation of L_1, we only take into account $\Delta\varphi_1=2\pi\mathrm{Re}(n_{\mathrm{eff}})\,(L_2-L_1)/\lambda$ (the variation of φ_1) for the fixed L. As L_1=90 nm, L=600 nm, Re(n_{eff})=1.26 and λ=550 nm, we have $\Delta\varphi_1=1.9244\pi\approx2\pi$. Substituting the above parameters into Eq. 6, we get the identical results to the case of $L_1=L_2$=300 nm ($\Delta\varphi_1$=0). So, the disappearance of TM_3 mode, for both L_1=300 and 90 nm, arises from $\Delta\varphi_1=2\pi\mathrm{Re}(n_{\mathrm{eff}})\,(L_2-L_1)/\lambda=2q\pi$ (q is an integer) when L is fixed at 600 nm. By comparing Fig. 2a with Fig. 2f, one can conclude that the theoretical model is consistent with the FDTD method and phase shifts (φ_1 and φ_2) in slot cavity contribute to the periodic variation of transmission dips in the plasmonic structure. Consequently, the theoretical analysis allows us to understand spectral responses of the plasmonic filter system as a function of their microscopic parameters.

Slowing down light in plasmonic structure induces enhanced light-matter interaction and therefore improves the performance of nanoscale plasmonic devices. Group index (n_g) in the plasmonic waveguide system can be calculated by the following formula [18, 36]:

$$n_{\mathrm{g}}=\frac{c}{v_{\mathrm{g}}}=\frac{c}{l}\tau_{\mathrm{g}}=\frac{c}{l}\frac{d\theta}{d\omega}, \tag{7}$$

where c is the speed of light in vacuum, τ_g is the optical delay time, θ is transmission phase shift, v_g stands for the group velocity, and l is the length of the plasmonic system. The dispersion of transmission phase shift versus L_1 and λ is plotted in Fig. 3a, which presents that there is a sudden phase jump around the transmission dip and the phase slope is negative with respect to λ. Figure 3b, c depicts the corresponding optical delay and group index of the plasmonic structure. The maximum optical delay (group index) around TM_4 and TM_3 modes, respectively, are 0.14 ps [35] and 0.12 ps [30]. Furthermore, the group index around TM_4 mode keeps nearly constant versus L_1 but varies periodically around TM_3 mode, which may be promising for the development of ultracompact optical buffers.

In Fig. 4a, we plot a series of transmission spectra versus the relative dielectric constant ξ_d in slot cavity with the other parameters fixed at w=100 nm, g=120 m, and $L_1=L_2$= 300 nm. Figure 4b shows the wavelength of transmission dips

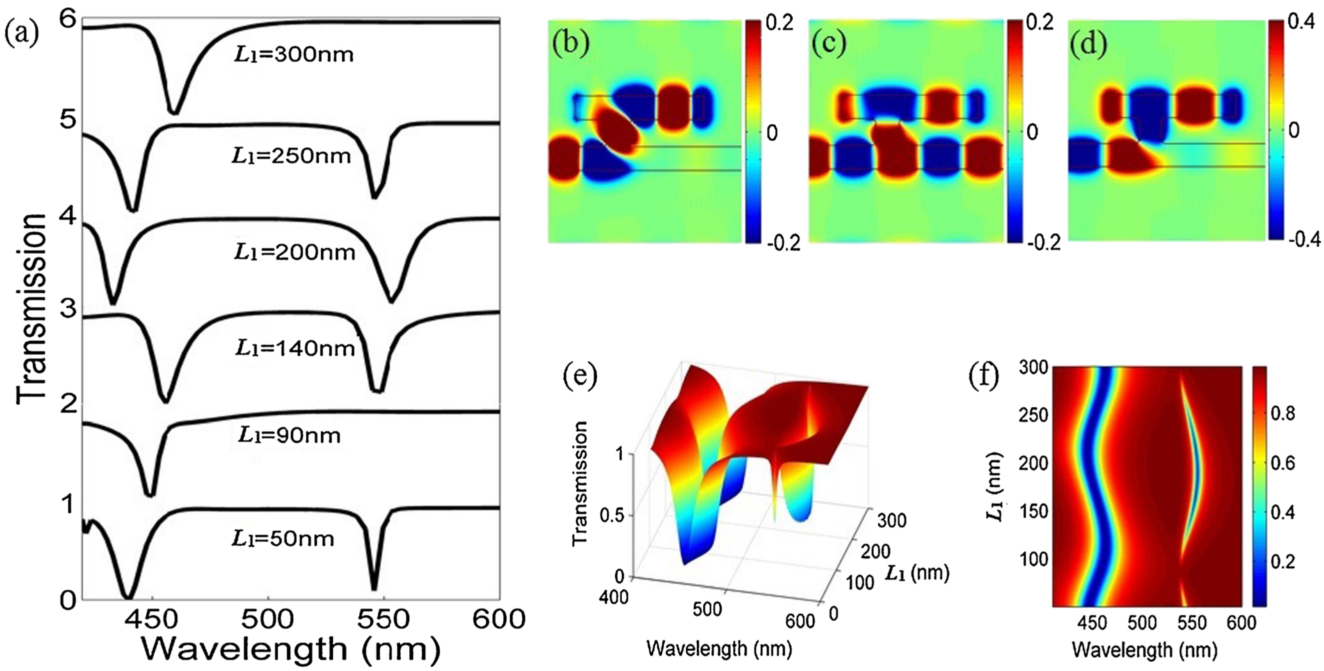

Fig. 2 **a** Transmission spectra with different L_1. Field distributions of H_z in the plasmonic filter at different wavelengths **b** λ=433 nm, **c** λ=553.3 nm, and **d** λ=781.2 nm. The other geometrical parameters are w=100 nm, g=120 nm, L_1=200 nm, and L=L_1 + L_2=600 nm. **e** Evolution of the transmission spectra versus L_1 and λ. **f** The top view of **e**

in Fig. 4a with ξ_d increasing from 1.0 to 1.6. The field distributions H_z at TM_{4N} mode exhibit 4 nodes in the slot cavity, yet with different patterns compared to TM_4 mode (not shown here). It is found that all the wavelengths of resonance modes present red shift and mode spacing increases linearly with the increase of ξ_d. In this case, due to L_1=L_2=$L/2$, Eq. 6 can be rewritten as

$$t=\frac{S_{-22}}{S_{+21}}=\frac{j\left(\frac{\omega}{\omega_0}-1\right)+\frac{1}{Q_i}+\frac{1}{2Q_1}-\frac{1}{Q_1}\frac{1}{1-\frac{e^{j\phi}}{\sigma}}}{j\left(\frac{\omega}{\omega_0}-1\right)+\frac{1}{Q_i}+\frac{1}{2Q_1}+\frac{1}{2Q_2}-\frac{1}{Q_1}\frac{1}{1-\frac{e^{j\phi}}{\sigma}}}. \tag{8}$$

Here, the phase term $\varphi=\varphi_1=\varphi_2=2\omega\mathrm{Re}(n_{\mathrm{eff}})L_1/c+\delta_1$. To investigate the transmission spectra in Fig. 4a more explicitly, the real of effective index $\mathrm{Re}(n_{\mathrm{eff}})$ [5, 18, 40] in the slot cavity (w=100 nm), as a function of relative dielectric constant ξ_d and incident light wavelength, is illustrated in Fig. 4c. As seen from Fig. 4c, $\mathrm{Re}(n_{\mathrm{eff}})$ increases apparently with the increase of ξ_d at a certain wavelength, while $\mathrm{Re}(n_{\mathrm{eff}})$, with ξ_d fixed, varies very slowly in the visible and near infrared. So, adjusting relative dielectric constant ξ_d is an effective way to manipulate the real of effective index $\mathrm{Re}(n_{\mathrm{eff}})$ in MDM structure and provides us a method to manipulate phase shifts (φ_1 and φ_2) in slot cavity to control the transmission responses. When the other geometrical and constitutive parameters are fixed, $\mathrm{Re}(n_{\mathrm{eff}})$ is only related to ξ_d at a certain wavelength. Based on Eq. 8, the evolution of transmission spectra versus $\mathrm{Re}(n_{\mathrm{eff}})$

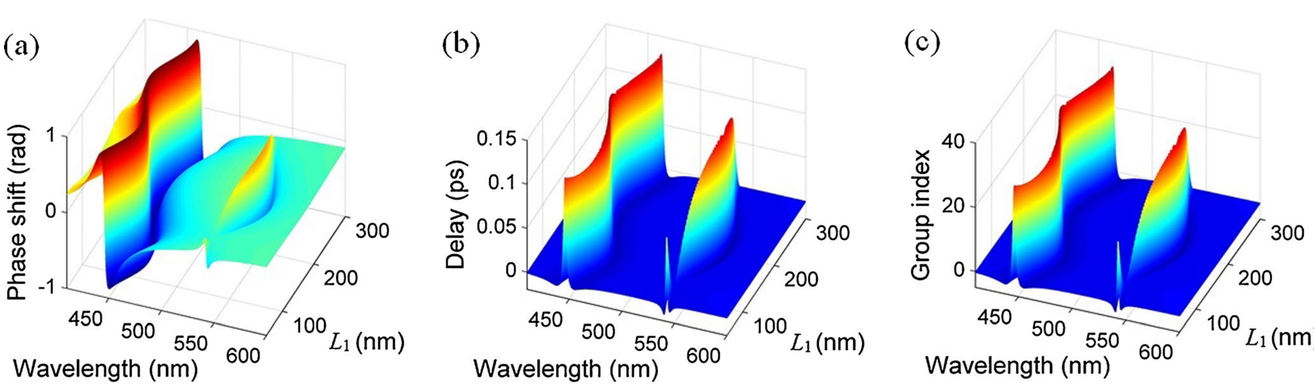

Fig. 3 Evolution of **a** transmission phase shift, **b** optical delay time, and **c** group index versus L_1 and λ

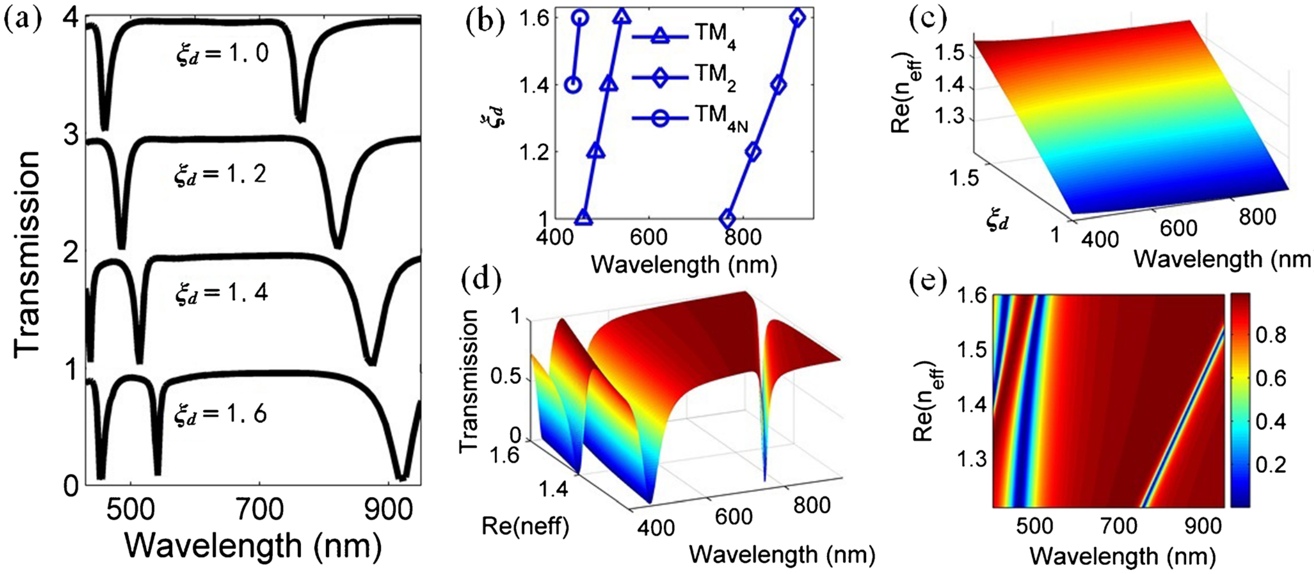

Fig. 4 **a** Transmission spectra for different relative dielectric constant ξ_d in the slot cavity. The other geometrical parameters are w=100 nm, g=120 m, and L_1=L_2=300 nm. **b** The wavelength of the transmission dips in **a** as a function of ξ_d. **c** Dependence of Re(n_{eff}) in slot cavity on the wavelength of incident light and the relative dielectric constant ξ_d. **d** Evolution of the transmission spectra versus Re(n_{eff}) and λ. **e** The top view of **d**

and λ is plotted in Fig. 4d, of which the top view is shown in Fig. 4e. We can see that the theoretical results are in good agreement with the FDTD simulations except for a little discrepancy of the FWHM of TM$_2$ mode, which is caused by the dispersion of n_{eff} and cavity quality factors (Q_i, Q_1, and Q_2). Combing Figs. 2f and 4e, we conclude that one could realize the required transmission spectra by tuning the phase shifts in slot cavity. Furthermore, from the analytical model, we also obtain that the increase of L_1 (ξ_d) will increase the sensitivity of transmission spectra to ξ_d (L_1) in the plasmonic structure with fixed L.

From Eqs. 6 and 8, it is clear that ω_0 (resonance frequency of the resonator shown in Fig. 2b) also affects the transmission properties. In Fig. 5a, the transmission spectra versus gap g are investigated by the FDTD simulations. The blue and red solid lines correspond to, respectively, the symmetric (L_1=L_2=300 nm, w=100 nm) and asymmetric structures (L_1=230 nm, L_2=370 nm, and w=100 nm). For both cases,

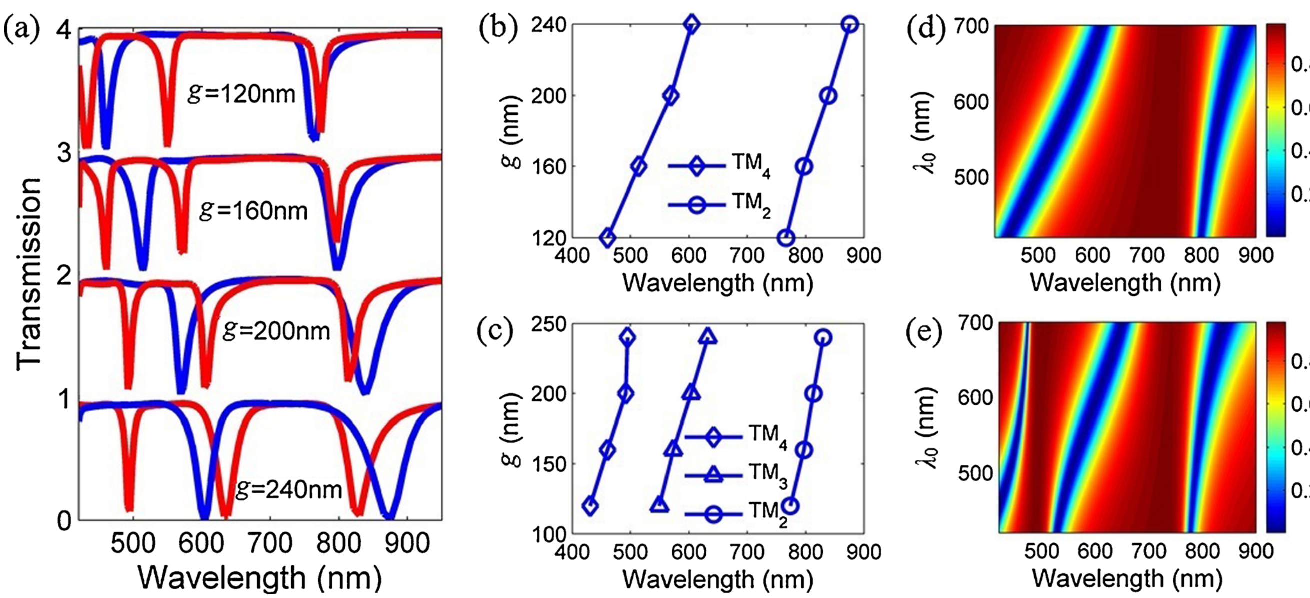

Fig. 5 **a** Transmission spectra versus different gap g for symmetric (*blue solid line*, L_1=L_2=300 nm, w=100 nm) and asymmetric (*red solid line*, L_1=230 nm, L_2=370 nm, and w=100 nm) structures. The wavelength of transmission dips in **a** as a function of g for **b** symmetric structure, and **c** asymmetric structure. Transmission spectra versus λ_0 (resonant wavelength of the resonator plotted in Fig. 2b) and incident light wavelength for **d** symmetric and **e** asymmetric structures

Fig. 5b, c shows that the transmission dips exhibit red shift with the increment of g. The resonance wavelength λ_0 (corresponding to ω_0) is determined only by g, as the other parameters are fixed. So, to investigate the evolution of transmission spectra versus g, in Fig. 5d, e, we plot the transmission spectra versus resonant wavelength λ_0 and incident light wavelength by the analytical model. The transmission spectra in Fig. 5d, e are in good accordance with those in Fig. 5a. For the symmetric case in Fig. 5b, d, the mode spacing between TM_4 and TM_2 modes becomes smaller for larger g, but TM_3 mode (odd mode) is suppressed, which is attributed to $\Delta\varphi_1 = 2\pi\mathrm{Re}(n_{\mathrm{eff}})\,(L_2 - L_1)/\lambda = 0$ and similar to the analysis based on the superposition principle of optics and cavity model [33]. For the asymmetric case in Fig. 5c, e, the mode spacing between TM_2 and TM_3 modes decreases with increasing g, while the mode spacing between TM_3 and TM_4 modes increases. As mentioned above, both the CMT and FDTD methods demonstrate the mode selectivity and filtering tunability of the plasmonic structure with the variation of g, which further verifies the feasibility of the theoretical analysis.

Conclusion

In summary, we have derived an analytical model, by taking the aperture as a resonator, for an ultracompact plasmonic filter based on aperture-side-coupled slot cavity. The filter responses obtained theoretically are in good agreement with the rigorous FDTD simulations. Both the theoretical analysis and numerical calculations demonstrate the mode selectivity and filtering tunability of the plasmonic structure. Using the analytical model, we manipulate the transmission properties via phase shifts (φ_1 and φ_2) of SPPs mode in the slot cavity and resonance frequency (ω_0) determined by the aperture, and can also predict the slow light effect. Importantly, the excitation of TM_3 mode (odd mode) for both the symmetric and asymmetric structures depends on whether the relation $\Delta\varphi_1 = 2\pi\mathrm{Re}(n_{\mathrm{eff}})\,(L_2 - L_1)/\lambda = 2q\pi$ (q is an integer) is satisfied or not. Moreover, the maximum optical delay (group index) around TM_4 and TM_3 modes are 0.14 ps (35) and 0.12 ps (30), respectively. The results, for the exact and systematic analysis of the selective-mode plasmonic filter, may provide an in-depth understanding of transmission in aperture-side-coupled nanostructure and have potential applications for wavelength-selective, plasmonic sensing, and slow light devices in plasmonic waveguide platforms.

Acknowledgments This work was funded by the Fundamental Research Funds for the Central Universities of Central South University under Grant No. 2012zzts007 and 2013zzts009, the Research Fund for the Doctoral Program of Higher Education of China under Grant No. 20100162110068, and the National Natural Science Foundation of China under Grant No. 61275174.

References

1. Bozhevolnyi SI (2009) Plasmonic nanoguides and circuits. Pan Stanford Publishing Pte. Ltd, Singapore
2. Pile DFP, Ogawa T, Gramotnev DK, Matsuzaki Y, Vernon KC, Yamaguchi K, Okamoto T, Haraguchi M, Fukui M (2005) Two-dimensionally localized modes of a nanoscale gap plasmon waveguide. Appl Phys Lett 87:261114
3. Chen JJ, Li Z, Zhang X, Xiao JH, Gong QH (2013) Submicron bidirectional all-optical plasmonic switches. Sci Rep 3:1451
4. Park JH, Kim KY, Lee IM, Na HM, Lee SY, Lee BH (2010) Trapping light in plasmonic waveguides. Opt Express 18:598–623
5. Economou EN (1969) Surface plasmons in thin films. Phys Rev 182: 539–554
6. Gramotnev DK, Bozhevolnyi SI (2010) Plasmonics beyond the diffraction limit. Nat Photonics 4:83–91
7. Leveque AG, Szunerits S, Pennec Y, Djafari-Rouhani B, Boukherroub R, Dobrzynski L (2013) Nanometal plasmon polaritons. Surf Sci Rep 68:1–67
8. Cai W, Shin W, Fan S, Brongersma ML (2010) Elementsfor plasmonic nanocircuits with three-dimensional slot waveguides. Adv Mater 22:5120–5124
9. Zhang X, Li Z, Chen JJ, Yue S, Gong QH (2013) A dichroic surface-plasmon-polariton splitter based on an asymmetric T-shape nanoslit. Opt Express 21:14548–14554
10. Chen JJ, Li Z, Yue S, Xiao JH, Gong QH (2012) Plasmon-induced transparency in asymmetric T-shape single slit. Nano Lett 12:2494–2498
11. Chheang V, Lee TK, Oh GY, Kim HS, Lee BH, Kim DG, Choi YW (2013) Compact polarizing beam splitter based on a metal-insulator-metal inserted into multimode interference coupler. Opt Express 21: 20880–20887
12. Lee TW, Gray S (2005) Subwavelength light bending by metal slit structures. Opt Express 13:9652–9659
13. Guo YN, Wang HN, Reed JM, Pan S, Zou SL (2013) Effective light bending and controlling in a chamber-channel waveguide system. Opt Lett 38:2209–2211
14. Gao H, Shi H, Wang C, Du C, Luo X, Deng Q, Lv Y, Lin X, Yao H (2005) Surface plasmon polariton propagation and combination in Y-shaped metallic channels. Opt Express 13:10795–10800
15. Veronis G, Fan S (2007) Theoretical investigation of compact couplers between dielectric slab waveguides and two-dimensional metal-dielectric-metal plasmonic waveguides. Opt Express 15:1211–1221
16. Rotenberg N, Beggs DM, Sipe JE, Kuipers L (2013) Resonant coupling from a new angle: coherent control through geometry. Opt Express 21:16504–16513
17. Wang B, Wang GP (2004) Surface plasmon polariton propagation in nanoscale metal gap waveguides. Opt Lett 29:1992–1994
18. Cao GT, Li HJ, Zhan SP, Xu HQ, Liu ZM, He ZH, Wang Y (2013) Formation and evolution mechanisms of plasmon-induced transparency in MDM waveguide with two stub resonators. Opt Express 21: 9198–9205
19. Chen L, Gao CM, Xu JM, Zang XF, Cai B, Zhu Y (2013) Observation of electromagnetically induced transparency-like transmission in terahertz asymmetric waveguide-cavities systems. Opt Lett 38:1379–1381
20. Piao XJ, Yu S, Park N (2012) Control of Fano asymmetry in plasmon induced transparency and its application to plasmonic waveguide modulator. Opt Express 20:18994–18999

21. Lu H, Liu XM, Mao D, Gong YK, Wang GX (2011) Induced transparency in nanoscale plasmonic resonator systems. Opt Lett 36:3233–3235
22. Intaraprasonk V, Fan SH (2012) Enhancing the waveguide-resonator optical force with an all-optical on-chip analog of electromagnetically induced transparency. Phys Rev A 86:063833
23. Lin XS, Huang XG (2008) Tooth-shaped plasmonic waveguide filters with nanometeric sizes. Opt Lett 33:2874–2876
24. Tao J, Huang XG, Lin X, Zhang Q, Jin X (2009) A narrow-band subwavelength plasmonic waveguide filter with asymmetrical multiple-teeth-shaped structure. Opt Express 17: 13989–13994
25. Pannipitiya A, Rukhlenko ID, Premaratne M, Hattori HT, Agrawal GP (2010) Improved transmission model for metal-dielectric-metal plasmonic waveguides with stub structure. Opt Express 18:6191–6204
26. Luo X, Zou XH, Li XF, Zhou Z, Pan W, Yan LS, Wen KH (2013) High-uniformity multichannel plasmonic filter using linearly lengthened insulators in metal–insulator–metal waveguide. Opt Lett 38: 1585–1587
27. Wen KH, Yan LS, Pan W, Luo B, Guo Z, Guo YH, Luo XG (2013) Design of plasmonic comb-like filters using loop-based resonators. Plasmonics 8:1017–1022
28. Lu H, Liu XM, Mao D, Wang LR, Gong YK (2010) Tunable band-pass plasmonic waveguide filters with nanodisk resonators. Opt Express 18:17922–17927
29. Rezaei M, Miri M, Khavasi A, Mehrany K, Rashidian B (2012) An efficient circuit model for the analysis and design of rectangular plasmonic resonators. Plasmonics 7:245–252
30. Yun BF, Hu GH, Cui YP (2013) Resonant mode analysis of the nanoscale surface plasmon polariton waveguide filter with rectangle cavity. Plasmonics 8:267–275
31. Zand I, Abrishamian MS, Berini P (2013) Highly tunable nanoscale metal-insulator-metal split ring core ring resonators (SRCRRs). Opt Express 21:79–86
32. Yu HC, Chen MH, Li PX, Yang SG, Chen HW, Xie SZ (2013) Compact Q-value enhanced bandpass filter based on the EIT-like effect accompanying application in downconversion APL. Opt Lett 38:3906–3909
33. Hu F, Yi H, Zhou Z (2011) Band-pass plasmonic slot filter with band selection and spectrally splitting capabilities. Opt Express 19:4848–4855
34. Han Z, Van V, Herman WN, Ho PT (2009) Aperture-coupled MIM plasmonic ring resonators with sub-diffraction modal volumes. Opt Express 17:12678–12684
35. Nielsen MP, Elezzabi AY (2013) Ultrafast all-optical modulation in a silicon nanoplasmonic resonator. Opt Express 21:20274–20279
36. Lu H, Liu XM, Mao D (2012) Plasmonic analog of electromagnetically induced transparency in multi-nanoresonator-coupled waveguide systems. Phys Rev A 85:053803
37. Han ZH, Bozhevolnyi SI (2011) Plasmon-induced transparency with detuned ultracompact Fabry-Perot resonators in integrated plasmonic devices. Opt Express 19:3251–3257
38. Haus HA (1984) Waves and fields in optoelectronics. Prentice-Hall, Englewood Cliffs, Chapter 7
39. Palik ED (1985) Handbook of optical constants of solids. Academic, Boston
40. Johnson PB, Christy RW (1972) Optical constants of the noble metals. Phys Rev B 6:4370–4379